27th International Congress on Sound and Vibration
The annual congress of the International Institute of Acoustics and Vibration (IIAV)
11-16 July, 2021
ICSV27
Annual Congress of the International Institute of Acoustics and Vibration (IIAV)

EXPERIMENTAL STUDY ON THE ACOUSTIC PROPERTIES OF PERFORATES UNDER FLOW USING THREE-PORT TECHNIQUE

Shail Shah, Hans Bodén and Susann Boij

KTH Royal Institute of Technology, Marcus Wallenberg Laboratory for Sound and Vibration Research, Stockholm, Sweden
email: shail@kth.se

The acoustic properties of a perforated plate are known to be dependent on, amongst other factors, the external flow. An ongoing scientific discussion is regarding the boundary condition of the perforated liners for acoustic propagation with different directions relative to the mean flow. This is due to the combination of these conditions resulting in varying acoustic properties of perforates, when evaluated by different impedance eduction measurement techniques. The work presented here is to contribute to the research and provide results for the acoustic behaviour of perforates under different flow conditions. A majority of the test rigs used to determine the acoustic impedance consider either upstream or downstream acoustic propagation in a two-port configuration. Here, a three-port measurement technique is used to observe the transfer impedance of the perforate using excitation from all the three directions. This setup allows for studying the effect of flow under grazing as well as normal acoustic incidence. Validation of the experimental results as well as comparison with existing analytical models to determine the transfer impedance of perforates are presented.
Keywords: Acoustic impedance, perforated plates, grazing flow

1. Introduction

Significant increase in domestic and international air travel over the past few decades has led to an increase in the research regarding noise reduction strategies involving aircraft noise. Fan noise, a major contributor, is acoustically treated using liners. Perforated and microperforated plates (MPPs) are essential components of these liners. Analytical and experimental research has been carried out on the potential and the behaviour of perforates since the 1950s [1]. Characterisation of the acoustic behaviour of liner face sheets is done using the transfer impedance. Since the important characteristic of a perforated face sheet is its 'lumpiness', i.e., its resistive nature, this study on perforated samples focuses only on the real part of the transfer impedance, i.e., the resistance. Experimental techniques developed for acoustic characterisation of liners depend on the test rig and eduction methods used [2]. In contrast to eduction methods, direct techniques like in-situ measurements [3] and an impedance tube in a sidebranch [4] have also been used to determine the properties of liners as well as of perforates. Direct techniques, along with the three-port technique described in this study, determine the impedance without using the Ingard-Myers boundary condition [5]. Hence, the contrariety about assuming this boundary condition should not be considered here.

The three-port determined here for acoustic characterisation of perforated samples is based on previously conducted experimental studies [6]. Based on the elements of the scattering matrix and the normalised particle velocity, the transfer impedance is determined. Validation of the calculated transfer imped-

ance is done by comparing results with two-port impedance tube measurements. Section 2 describes the techniques and formulations used in this study along with the proposed modifications. The transfer impedance results for both the two-port and the three-port experiments along with results showing the effect of grazing flow are presented in Section 3. Moreover, the behavioural trends of the resistance is compared with results from existing models [7-9].

2. Experimental Techniques

2.1 Impedance Tube and 2-Port Technique

The transfer impedance of the perforate sample was first estimated using two-port measurements conducted in an impedance tube. The schematic of the tube, the formulation of the two-port scattering matrix, (S-Matrix) as well as the notation and sign convention used are as shown in Figure 1.

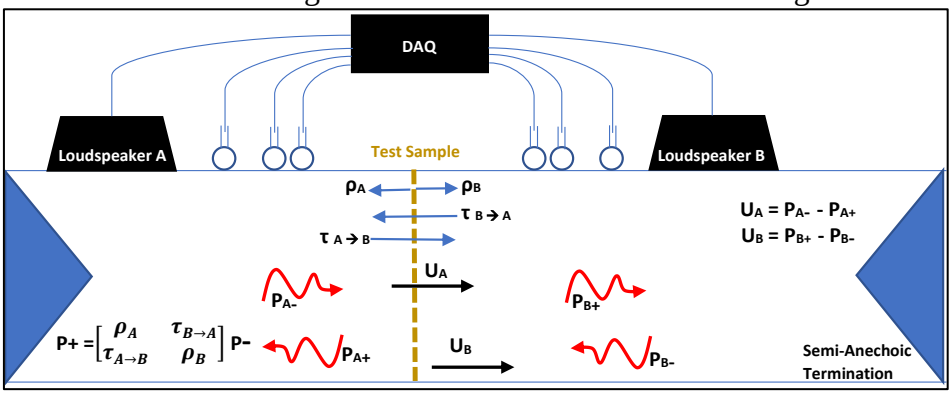

Figure 1 Schematic of impedance tube for two-port measurements

The wave decomposition and determination of the S-Matrix was carried out using the multi-microphone method [10] in the plane wave frequency range.

The actual transfer impedance of the sample and the particle velocity in direction normal to the sample surface was divided by the characteristic impedance of air to give the normalised transfer impedance ($\overline{Z}$) and the normalised particle velocity (u), respectively. Calculation of $\overline{Z}$ was done adhering to the following boundary conditions in this study:

- $\overline{Z}$ is defined as the difference between the normalised impedance on each side of the perforate following the equation:

$$\overline{Z} = \mathrm{Z_A} - Z_B = \frac{P_A}{u_A} - \frac{P_B}{u_B} = \frac{P_{A+} + P_{A-}}{u_A} - \frac{P_{B+} + P_{B-}}{u_B}, \tag{1}$$

  where $P_{A,B}$ describes the total pressure on the sample surface on each side of the sample, $P_{A\pm,B\pm}$ represent the decomposed components of the pressure wave and u, the total normalised particle velocity at the sample surface. The propagation directions are as per Figure 1. As the S-Matrix coefficients represent the acoustic properties of the sample independent of the reflection from the termination, we can consider Eq. (1) for anechoic termination i.e., $P_{B-} = 0$ when loudspeaker A is active. The reflection (ρ) and transmission (τ) coefficients of the test sample replace P_{A+} and P_{B+} in Eq. (1) and taking $P_{B-} = 0$ we can define $\overline{Z}$ as per Eq. (2). It should be noted that due to the symmetry of the sample, the same equation will hold when excitation is from loudspeaker B.

$$\overline{Z} = \frac{1+\rho_A}{1-\rho_A} - 1 = \begin{Bmatrix}\text{geometrical}\\ \text{symmetry}\end{Bmatrix} = \frac{1+\rho_B}{1-\rho_B} - 1 \tag{2}$$

- Given that the test sample is acoustically compact, $\overline{Z}$ can also be determined by taking the ratio of pressure difference across the sample and u. Particle velocity was calculated before and after the

sample, and either can be used to determine the impedance using the following equations:

$$\overline{Z} = \frac{P_A - P_B}{u_A} = \left\{\begin{matrix}\text{replacing } P_{A+} \text{and } P_{B+} \\ \text{with } \rho, \tau \text{ and } P_{B-} = 0\end{matrix}\right\} = \frac{1 + \rho_A - \tau_{A\to B}}{1 - \rho_A}$$
$$\overline{Z} = \frac{P_A - P_B}{u_B} = \left\{\begin{matrix}\text{replacing } P_{A+} \text{and } P_{B+} \\ \text{with } \rho, \tau \text{ and } P_{B-} = 0\end{matrix}\right\} = \frac{1 + \rho_A}{\tau_{A\to B}} - 1 \quad (3)$$

- Lastly, as the transfer impedance should be independent of termination, taking $Z_B = 0$ and by extension, $P_B = 0$ can also be considered as a boundary condition, leading to $P_{B+} = -P_{B-}$ and the following:

$$\overline{Z} = \frac{P_A - P_B}{u_A} = \frac{P_{A+} + P_{A-}}{P_{A-} - P_{A+}} = \frac{(1+\rho_B)(1+\rho_A) - \tau_{A\to B}\tau_{B\to A}}{(1+\rho_B)(1-\rho_A) + \tau_{A\to B}\tau_{B\to A}}$$
$$\overline{Z} = \frac{P_A - P_B}{u_B} = \frac{P_{A+} + P_{A-}}{P_{B+} - P_{B-}} = \frac{(1+\rho_B)(1+\rho_A) - \tau_{A\to B}\tau_{B\to A}}{2\tau_{A\to B}} \quad (4)$$

Theoretically, Eq. (1) to (4) should give the same results provided that $u_A = u_B$. However, due to measurement errors, experimentally determined particle velocities on each surface of the sample deviated by ≈2%. This resulted in a maximum deviation of ≈5% in the calculated transfer impedance. To determine the boundary condition defining the calculation of transfer impedance for the rest of this study, a variance-based fit was evaluated. The resulting curves of $\overline{Z}$ calculated using the above mentioned boundary conditions were compared. The boundary condition with the best fit (highest value of coefficient of determination R^2) between the results calculated using direct methods and the ones using equivalent S-Matrix formulations was selected, namely Eq. (3) with u_B.

An analytical model to determine the transfer impedance, based on viscous dissipation on both ends of the perforate holes was proposed by Guess [7]. Additionally, using the discharge coefficient was proposed by Elnady [9]. A combined model was found to fit the measurement results and is depicted by:

$$\Re = \frac{\sqrt{8\nu\omega}t'}{\sigma c d C_D}, t' = t + d, \quad (5)$$

where $\Re$ is the resistance (real part of $\overline{Z}$), ν is the kinematic viscosity, ω the angular frequency, d is the diameter of perforation, σ is the porosity, C_D is the discharge coefficient and t is the thickness of the sample. Here, t' is the corrected length of holes proposed by Guess [7]. This corrected length is equal to the sum of the sample thickness t and the end correction (in [7] equal to d).

2.2 Three Port Technique

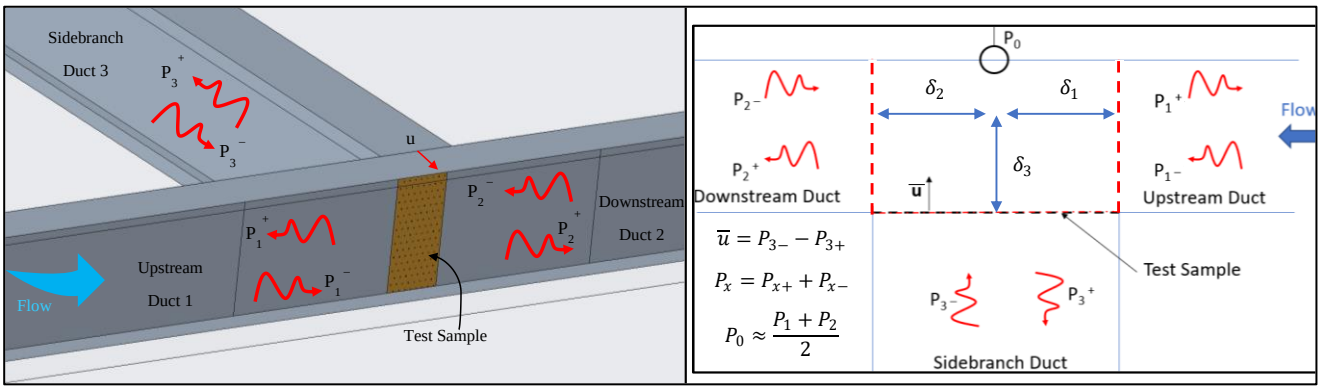

Figure 2 Schematic test setup for Three-port technique

The three-port setup from Holmberg et al [10] is realised by placing the test sample in the T-Junction, as shown in Figure 2. The end of Duct 3 was sealed, so that in presence of external grazing flow there is no mean flow in the sidebranch. Acoustic pressure is measured in all three duct parts and decomposed using the multi-microphone method. Moreover, the total acoustic pressure at the middle of the test sample on the opposite wall was measured using a flush mounted microphone (pressure P_0). When comparing the results, it was found that the average of the decomposed wave pressures in the upstream and downstream duct was equal to the measured pressure P_0 (maximum deviation < 5%).

It is necessary to define a physical point in the setup where the three-port collapses. An obvious choice is the centre of the perforate. However, Holmberg et al [10] proposed an addition of certain distances from the geometric centre for an empty T-Junction (no perforate) by comparing the phase angles of the transmission coefficients with each other. A modification of that method is used for a T-Junction containing a perforate, and the following equation was used to determine the alterations that need to be added to the geometric length:

$$-2\left(\delta_i + \delta_j\right) = c\, mean\left(\frac{\Delta\theta(\tau_{ij}) + \Delta\theta(\tau_{ji})}{2\pi f}\right), (i \neq j), \tag{6}$$

where i, j represent the ducts, $\delta_{i,j}$ are the added alterations for the respective ducts and $\Delta\theta(\tau_{ij,ji})$ is the deviation of the phase angle of the transmission coefficients when compared with the respective elements of the S-Matrix in the impedance tube results. In case of plane wave propagation, as per Holmberg et al [10], the value of the alteration should remain constant across the frequency range. Experimentally however, a deviation of <7% of its mean value was observed across the frequency range.

The S-Matrix for the three-port was determined using the following equation:

$$\begin{bmatrix} P^I_{1+} & P^{II}_{1+} & P^{III}_{1+} \\ P^I_{2+} & P^{II}_{2+} & P^{III}_{2+} \\ P^I_{3+} & P^{II}_{3+} & P^{III}_{3+} \end{bmatrix} = \begin{bmatrix} \rho_1 & \tau_{2\to1} & \tau_{3\to1} \\ \tau_{1\to2} & \rho_2 & \tau_{3\to2} \\ \tau_{1\to3} & \tau_{2\to3} & \rho_3 \end{bmatrix} \begin{bmatrix} P^I_{1-} & P^{II}_{1-} & P^{III}_{1-} \\ P^I_{2-} & P^{II}_{2-} & P^{III}_{2-} \\ P^I_{3-} & P^{II}_{3-} & P^{III}_{3-} \end{bmatrix}, or\ P^+ = SP^-, \tag{7}$$

where the numerical subscript refers to the duct number and the superscripted roman numerals represent the measurements carried out with excitation from Duct 1, 2 and 3, respectively. The normalised transfer impedance was calculated using direct methods and the S-Matrix coefficients. The formulas considered are based on Eq. (3):

$$\overline{Z} = \frac{\Delta P}{\overline{u}} = \frac{P_3 - P_0}{P_{3-} - P_{3+}}, \tag{8}$$

$$\overline{Z_1} = -1 + \frac{(\rho_1 + \tau_{1\to2} + 1)}{2\tau_{1\to3}}, \qquad \overline{Z_2} = -1 + \frac{(\rho_2 + \tau_{2\to1} + 1)}{2\tau_{2\to3}},$$
$$\overline{Z_3} = \frac{\rho_3 + 1}{-\rho_3 + 1} - \frac{1}{2}\frac{(\tau_{3\to1} + \tau_{3\to2})}{-\rho_3 + 1}, \tag{9}$$

where the directions are as shown in Figure 2 and Eq. (7). The subscript of $\overline{Z}$ represents the direction of excitation incidence.

Measurements were also carried out in the presence of grazing flow. Similar to Kooi and Sarin [8], the main flow parameter to be considered was the skin friction velocity (u_τ). Semi-empirical models proposed by Kooi and Sarin [8] and Cummings [11] depict normalised resistance as a function of u_τ and frequency (f). The Kooi and Sarin [8] model follows the equation:

$$\Re = \left(\frac{5 - {}^{t}/_{d}}{4\sigma c}\right)(9.9u_\tau - 3.2fd) \tag{10}$$

With another modelling approach, depending on the development of the flow boundary layer, Elnady [9] summarised models which describe the normalised resistance as only the function of mean Mach No. (M) and porosity (σ). This relation as described in Eq. (11):

$$\Re = \frac{\kappa M}{\sigma}, \tag{11}$$

where κ is a constant derived based on measurement results (κ = 0.5 for Elnady [10]).

Lee and Ih [12] proposed calculation of u_τ using mean grazing flow velocity ($u_{grazing}$), whereas Zanoun [13] proposed calculating it using the bulk velocity (u_{bulk}) as shown in Eq. (12) and (13), respectively.

$$Re_m = \frac{u_{grazing} * H}{\nu};\ u_\tau = \frac{u_{grazing}\sqrt{0.153\ (Re_m)^{-0,25}}}{2} \tag{12}$$

$$Re_m = \frac{u_{bulk} * H}{\nu};\ u_\tau = \frac{u_{bulk}\sqrt{0.0743\ (Re_m)^{-0,25}}}{2}, \tag{13}$$

where Re_m is the Reynolds Number calculated using the width of the duct (H). Due to discrepancies between the determined values of u_τ using Eqs. (12) and (13), a detailed flow profile measurement is required to correctly determine the skin friction velocity. Hence in this study, rather than comparing measured resistance against models mentioned in the above equations, only the trends of the curves, such as frequency dependence, will be discussed.

The test sample under consideration was a square-edged perforated plate with a thickness and diameter of perforation of 1.2mm each. The porosity of the measured sample was 2.5%. All measurements were performed at room temperature with deviation in the speed of sound <0.1%. The frequency range of the measurements was from 300-1500Hz. Wave numbers considered for the plane wave decomposition were calculated using a model proposed by Dokumaci [14]. The grazing flow velocity was measured using a pitot-static tube at the centre of the cross-section. Stepped sine excitation was used as input and reference signal. The frequency response function (FRF) between the measured pressure signal and the reference signal was used for the entire analysis to reduce measurement errors due to external noise.

3. Results

3.1 Impedance Tube Results

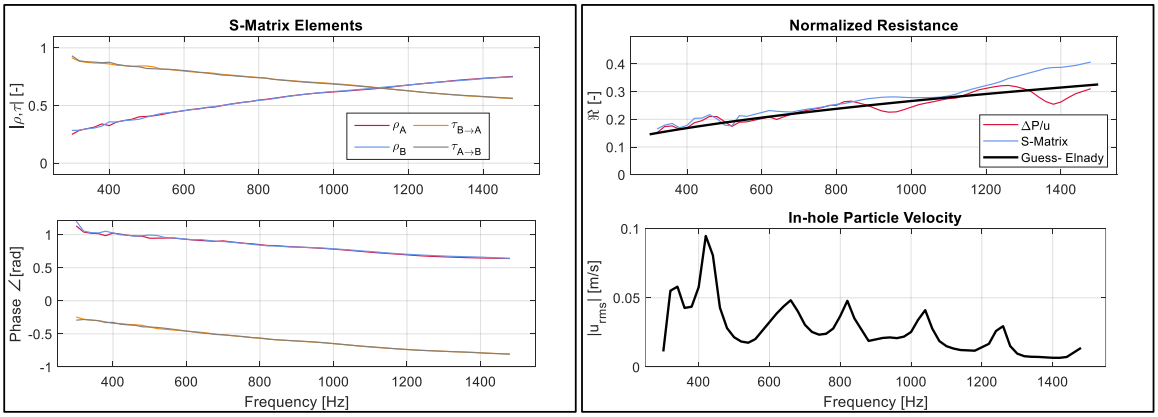

Figure 3 **(a)**: Magnitude and Phase Angles of S-Matrix Elements; **(b)**: Normalised Resistance calculated using formulas of Eq. (3) and (5), respectively and in-hole particle velocity.

As shown in Figure 3 and using the technique explained in Section 2.1, the S-Matrix coefficients and

the normalised resistance were calculated and compared with the model in Eq. (5). The value of C_D for the plate was taken equal to 0.76 as per Motsinger [15].

The reflection and transmission coefficient curves suggests that for low frequency, the perforate is comparatively acoustically transparent. This transparency is also observed in the resistance curves and occurs as the thickness of the perforate is small when compared with the excitation wavelength. A good agreement between the proposed model (Eq. (5)) and experimental results is also obtained up to around 1150Hz. Moreover, the resistance determined using the S-Matrix coefficients and direct methods also agrees well with an R^2 value of 0.97.

3.2 Three Port No Flow Results

Experiments were also performed in the T-Junction setup shown in Figure 2. As explained in Section 2.2, alterations were calculated to shift the centre-point of the sample and find a point where the three-port is chosen to collapse. The phase angle of the transmission coefficients to and from Duct 3 are compared with the results from the impedance tube measurements presented in section 3.1. The effect of considering these alterations on the resistance calculated under normal incidence along with the comparison with impedance tube results is as shown in Figure 4. On considering the alterations, results from the three-port match with those of the impedance tube and the model described in Eq. (5).

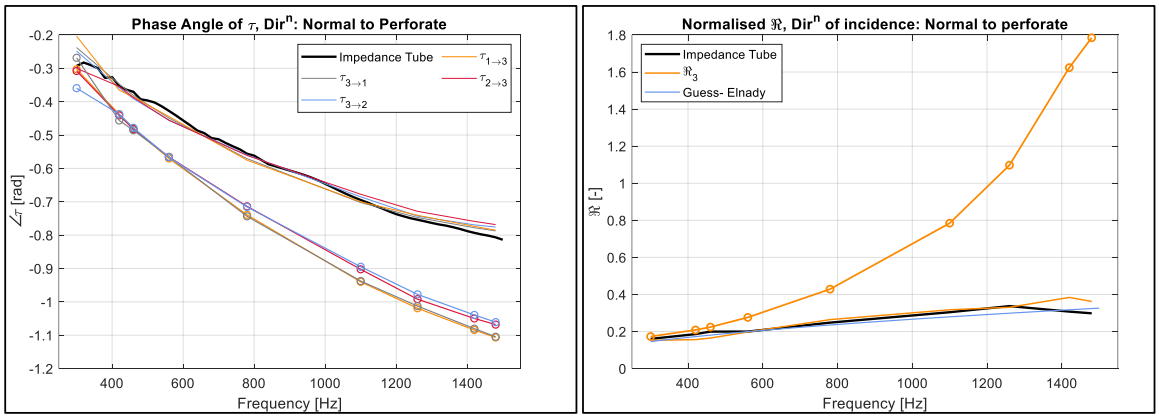

Figure 4 Comparison of calculated results of with **(solid lines)** and without **(circles)** altered lengths. **(a)**: Phase angles of transmission coefficients, **(b)**: Normalised resistance.

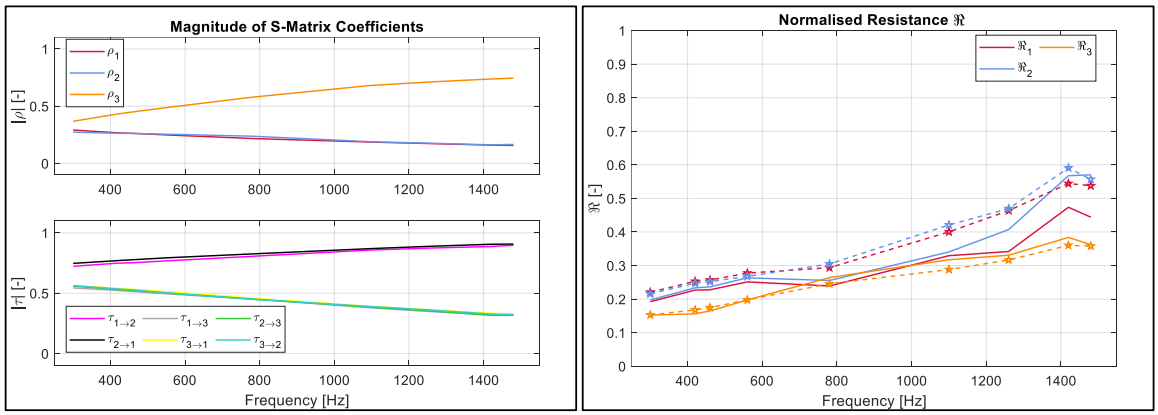

Figure 5 **(a)**: Magnitude of S-Matrix Coefficients, **(b)**: Normalised Resistance calculated using Eq. (8) **(solid lines)** and Eq. (9) **(pentagrams)**

The comparison between the measured resistance using independent excitations from all three ducts and the two methods stated in Section 2.2 is shown in Figure 5. The subscripts in the S-Matrix coefficients represent the duct number in Figure 5-a, and subscripts of $\Re$ in Figure 5-b represent the duct from where

the excitation is incident on the sample. Symmetry across Ducts 1 and 2 can be clearly observed in the S-Matrix coefficients as well as in the resistance curves. Deviations in the values under different incidence directions can be due to differences in the values of length alterations across the frequency range.

3.3 Three Port with Grazing Flow Results

The normalised resistance of the sample and the sound field in the ducts was then determined experimentally under the effect of grazing flow and the results are shown in Figure 6. The flow velocity was controlled to give the mean grazing Mach numbers of $M \approx 0.05$, 0.1, 0.15 and 0.2. Excitation from all the ducts is compared and the resistance is observed to be increasing with an increase in flow speed. In case of normal incidence, the resistance is found to decrease with increasing frequency, and remains directly proportional to grazing flow speed and consequently u_τ, following the model in Eq. (10). For flow speeds of $M > 0.1$ and under grazing incidence, the resistance becomes independent of the frequency, following the model in Eq. (11).

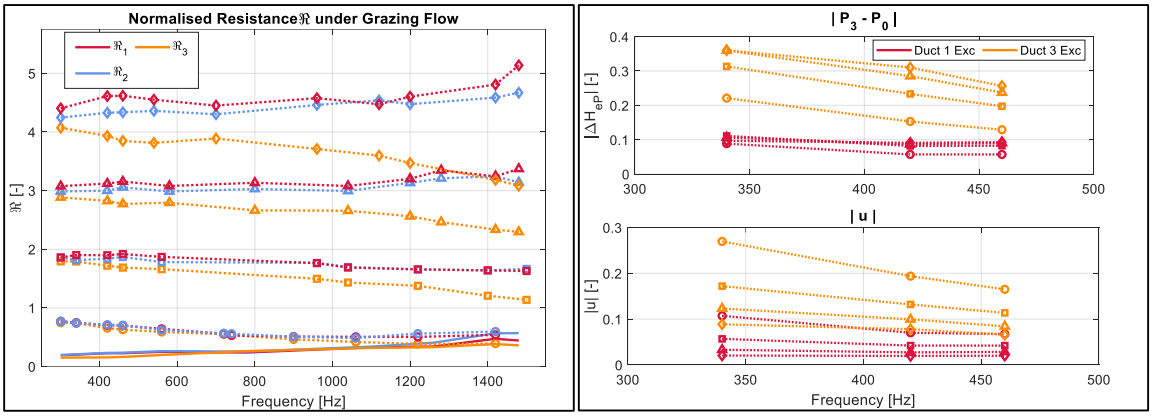

Figure 6 Perforate properties under external grazing flow of $M = 0$ **(solid lines)**, 0.05 **(circles)**, 0.1 **(squares)**, 0.15 **(triangles)** and 0.2 **(diamonds)**; **(a)** Normalised Resistance, **(b)** Magnitude of (i) FRF depicting acoustic pressure difference across the sample and (ii) normalised particle velocity for excitation from Duct 1 and Duct 3.

To study the behaviour of resistance under different incidence directions, the sound field is presented in Figure 6-b .The difference of the total pressure measured on each side of the perforate along with the particle velocity at the sample depict the sound field in both ducts. As mentioned in Section 2, the FRF between the pressure signal and the reference signal are used to depict the total acoustic pressure. Comparison till the frequency of 460 Hz is used to represent the behaviour over the entire frequency range.

On observing the sound field, it can be said that under normal incidence and increasing external flow speeds the particle velocity decreases. Moreover, this reduction in particle velocity is met with an increase in the pressure difference across the sample. Under grazing acoustic incidence, with an increase in grazing flow speeds, although a similar decrease in the particle velocity is observed, the increase in pressure difference is smaller. This difference in the behaviour of the sound field under different directions of acoustic incidence results in the deviation of the resistance curves at flow speeds of $M \geq 0.1$. However, the physical reason for this difference in behaviour remains to be explained.

At a comparatively low flow speed of $M \approx 0.05$, this deviation in the resistance curves is not observed. Moreover, in case of grazing incidence a decrease in the pressure difference was observed over the entire frequency range (in Figure 6-b at 420 Hz). At lower flow speeds, the acoustic field (thermo-viscous dissipation) as expected, influences the nature of resistance of the perforate. However, at higher flow speeds the behaviour is dominated by the flow field, with a frequency dependence that is different for normal and grazing acoustic incidence. In Bodén et al [16] a difference in the behaviour of resistance was observed in case of grazing acoustic incidence with respect to the direction of the external flow, i.e., when the acoustic incidence is in- and against the direction of flow, the resistance follows the model in

Eq. (10) and Eq. (11), respectively. No such variation in resistance is observed in the results in this study.

4. Conclusion

The study presents usage of a three-port technique to determine the resistance of perforates. Validation of the measured results is done by comparing with traditional two-port measurements. Formulas are proposed to calculate the transfer impedance using the S-Matrix coefficients as well as a comparison between existing impedance models is done with good agreement between all results. The resistance was also studied under the effect of external flow and depending on the characteristics of the flow profile, like skin friction velocity and mean flow speed, its properties were studied. Moreover, the dependence of resistance on the direction of acoustic incidence was presented by showing a difference in the frequency dependency of the resistance under normal and grazing acoustic incidence. Future works include quantification of this behaviour in terms of flow profile and perforate characteristics.

ACKNOWLEDGMENTS

This work is part of the Marie Skłodowska-Curie Initial Training Network **Pol**lution **K**now-How and **A**batement (POLKA). We gratefully acknowledge the financial support from the European Commission under call H2020-MSCA-ITN-2018 (project number: 813367).

REFERENCES

1. Ingård, U., *On the theory and design of acoustic actuators.* Journal of the Acoustical Society of America, 1953. **25**: p. 1037-1061.
2. Jones, M.G. , Watson, W.R., Howerton, B.M. and Busse-Gerstengarbe, S., *Comparative study of Impedance Eduction Methods, art 2: NASA Tests and Methodology*, in *19th AIAA/CEAS Aeroacoustics Conference*. 2013.
3. Dean, P.D., *An In-Situ method of wall acoustic impedance measurements in flow ducts.* Journal of Sound and Vibration, 1974. **34**: p. 97-130.
4. Dickey, N.S., Selamet, A. and Ciray, M.S., *An experimental study of the impedance of perforated plates with grazing flow.* Journal of Acoustical Society of America, 2001. **110**: p. 2360-2370.
5. Myers, M.K., *On the Acoustic Boundary Condition in the presence of Flow.* Journal of Sound and Vibration, 1980. **71**: p. 429-434.
6. Karlsson, M. and Åbom, M., *Aeroacoustics of T-junctions-an experimental investigation.* Journal of Sound and Vibration, 2010. **329**: p. 1793-1808.
7. Guess, A.W., *Calculation of Perforated Plate Liner Parameters from Specified Acoustic Resistance and Reactance.* Journal of Sound and Vibration, 1975. **40**: p. 119-137.
8. Kooi, J.W. and Sarin, S.L., *An experimental study of the acoustic impedance of Helmholtz resonator arrays under a turbulent boundary layer*, in *7th AIAA Aeroacoustics Conference*. 1981.
9. Elnady, T. and Bodén, H. *On the modelling of the acoustic impedance of perforates with flow*. in *9th AIAA/CEAS Aeroacoustics Conference*. 2003.
10. Holmberg, A., Karlsson, M. and Åbom, M., *Aeroacoustics of rectangular T-junctions subject to combined grazing and bias flows - An experimental investigation.* Journal of Sound and Vibration, 2015. **340**: p. 152-166.
11. Cummings, A., *The effects of Grazing Turbulent Pipe-Flow on the Impedance of an Orifice.* Acoustica, 1986. **61**: p. 233-242.
12. Lee, S-H. and Ih, J-G., *Empirical model of the acoustic impedance of a circular orifice in grazing mean flow.* Journal of Acoustical Society of America, 2003. **114**: p. 98-113.
13. Zanoun, E-S, Nagib,H. and Durst, F., *Refined cf relation for turbulent channels and consequences for high-Re experiments.* Fluid Dynamics Research, 2009. **41**.
14. Dokumaci, E., *A Note on Transmission of Sound in a Wide Pipe with Mean Flow and Viscothermal Attenuation.* Journal of Sound and Vibration, 1997. **208**: p. 653-655.
15. Motsinger, R.E. and Kraft, R.E., *Design and performance of duct acoustic treatment*, in *Aeroacoustics of Flight Vehicles*. 1991, NASA.
16. Bodén, H., Zhou, L., Cordioli, J., Medeiros, A. and Spillere, A., *On the effect of flow direction on impedance eduction results*, in *22nd AIAA Aeroacoustics Conference*. 2016.